

# C electro sorption on Ag(100): Lateral interactions and electro sorption valency from comparison of Monte Carlo simulations with chronocoulometry experiments

I. Abou Hamad<sup>1;2</sup>, S.J.M. Itchell<sup>3;4</sup>, Th. W andlow ski<sup>5</sup>, P.A.R.ikvold<sup>1;2</sup>, and G.Brown<sup>2;6</sup>

<sup>1</sup>Center for Materials Research and Technology and Department of Physics, Florida State University, Tallahassee, FL 32306-4350, USA

<sup>2</sup>School of Computational Science, Florida State University, Tallahassee, FL 32306-4120, USA

<sup>3</sup>Schuit Institute for Catalysis and Department of Chemical Engineering, Eindhoven University of Technology, 5600 MB Eindhoven, The Netherlands

<sup>4</sup>The Center for Computational Physics and The Department of Physics and Astronomy, The University of Georgia, Athens, GA 30602-2451

<sup>5</sup>Institute for Thin Films and Interfaces, ISG 3, and Center of Nanoelectronic Systems, cni, Research Centre Jülich, 52425 Jülich, Germany

<sup>6</sup>Center for Computational Sciences, Oak Ridge National Laboratory, Oak Ridge, TN 37831, USA

February 8, 2020

## Abstract

We present Monte Carlo Simulations using an equilibrium lattice-gas model for the electro sorption of Cl on Ag(100) single-crystal surfaces. Fitting the simulated isotherms to chronocoulometry experiments, we extract parameters such as the electro sorption valency and the next-nearest-neighbor lateral interaction energy  $\epsilon_{nnn}$ . Both coverage-dependent and coverage independent  $\epsilon_{nnn}$  were previously studied assuming a constant  $\epsilon_{nnn}$  [I. Abou Hamad, Th. W andlow ski, G. Brown, P.A.R.ikvold, *J. Electroanal. Chem.* 554-555 (2003) 211]. Here, a self-consistent, entirely electrostatic picture of the lateral interactions with a coverage-dependent  $\epsilon_{nnn}$  is developed, and a relationship between  $\epsilon_{nnn}$  and  $\epsilon_{nn}$  is investigated for Cl on Ag(100).

**Keywords:** Chlorine electro sorption; Lateral interactions; Electro sorption valency; Chronocoulometry; Continuous phase transition; Lattice-gas model; Monte Carlo simulation.

## 1 Introduction

Studies of lateral interactions between adsorbed particles are motivated by the need to understand the origin of the wide variety of ordered overlayers and phase transitions at fractional adsorbate coverage on metal surfaces. These interactions have contributions ranging from short-range and van der Waals to long-range dipole-dipole, and lattice-mediated interactions [1]. Hard-square short-range interactions and dipole-dipole long-range interactions are the major contributions to the lateral interactions for bromine adsorption on Ag(100) [2]. In this paper, we explore the validity and applicability of such a model for adsorption of chlorine on Ag(100).

Halide electrosorption on single-crystal metal electrode surfaces is a good model system for studying the properties of the electrode-electrolyte interface in an electrochemical cell. Due to its relative simplicity, it can be used to distinguish between the various contributions of different parameters according to the effect of their inclusion on the overall behavior of the system. A mean-field approach is not sufficient, even for the description of one of the simplest halide-electrosorption systems Br/Ag(100). However, a simple lattice-gas model with constant parameters is sufficient to describe its equilibrium [2, 3], and dynamic [4] properties. While the electrosorption of Br on single-crystal Ag(100) from aqueous solution has been extensively studied as an example of a layer formation in an electrochemical system [2, 5, 6, 7, 8], less attention has been given to the electrosorption of Cl [3, 9, 10] on Ag(100). A lattice-gas model with constant parameters is not sufficient to describe Cl/Ag(100), therefore this system can be used to further investigate the nature and characteristics of the lateral interactions between the adsorbed halide atoms. In particular, we here develop a self-consistent picture of variable lattice-gas parameters based on the resident charge on the adatoms being coverage dependent or electrode-potential dependent (through the coverage).

The rest of this paper is organized as follows. In Section 2 we describe an electrostatic model of the adlayer that is used in the simulations, the lateral interaction energies, and the Monte Carlo methods used. A brief description of the experimental procedure is given in Section 3. The results of fitting the simulations to experimental data are detailed in Section 4, followed by conclusions in Section 5.

## 2 Self-consistent electrostatic adlayer model

### 2.1 Lattice-gas model

The adsorption of Cl<sup>-</sup> ions occurs at the fourfold hollow sites of the Ag(100) surface [11], which form a square lattice as shown in Fig. 1. To approximate the equilibrium behavior of this system, we use a lattice-gas model, in which the lattice sites correspond to the adsorption sites. Mitchell et al. [12] used an  $\alpha$ -lattice model for the Br/Ag(100) system to show that the Br adsorbates spend most of the time near the four-fold hollow sites of the Ag(100) surface, thus justifying the lattice-gas treatment of halide adsorption. To describe the energy associated with a conformation of adsorbates on the surface, a grand-canonical effective Hamiltionian [2, 6, 13, 14] is used,

$$H = \sum_{i < j}^{N^2} \epsilon_{ij} c_i c_j - \frac{N}{2} \bar{\epsilon} c_i; \quad (1)$$

where  $\sum_{i < j}^N$  is a sum over all pairs of sites,  $\epsilon_{ij}$  are the lateral interaction energies between particles on the  $i$ th and  $j$ th lattice sites, measured in meV/pair,  $\bar{\epsilon}$  is the electrochemical potential, measured in meV/particle, and  $N = L^2$  is the total number of lattice sites. The local occupation variable  $c_i$  is 1 if site  $i$  is occupied and 0 otherwise.

The long-range interactions,  $\epsilon_{ij}$ , depend on the distance,  $r_{ij}$ , between ions  $i$  and  $j$  (measured in Ag(100) lattice spacing units,  $a = 2.889 \text{ \AA}$  [7]) as

$$\epsilon_{ij} = \begin{cases} 1 & r_{ij} = 1 \\ \frac{1}{2^{3/2} r_{ij}^{3/2}} & r_{ij} > 1 \end{cases}; \quad (2)$$

where the infinite value for  $r_{ij} = 1$  indicates nearest-neighbor exclusion, and negative values of  $\epsilon_{ij}$  denote long-range repulsion. The coverage isotherms were simulated using a square  $L \times L$  lattice with periodic boundary conditions to reduce finite-size effects.

The electrochemical potential  $\bar{\epsilon}$  is related to the bulk ionic concentration  $C$  and the electrode potential  $E$  (measured in mV). In the dilute-solution approximation, the relationship is

$$\bar{\epsilon} = \bar{\epsilon}_0 + k_B T \ln \frac{C}{C_0} e^{\frac{Z}{k_B T} (E - E_0)}; \quad (3)$$

where  $\bar{\gamma}_0$  is an arbitrary constant,  $C_0$  is a reference concentration (here taken to be 1 m M), and  $e$  is the elementary charge unit [15]. The reference potential  $E_0$  is chosen sufficiently negative such that the coverage vanishes at  $E_0$  for all values of  $C$  used, and  $\bar{\gamma}$  has the sign convention that  $\bar{\gamma} > 0$  favors adsorption. The relationship between  $\bar{\gamma}$ ,  $C$ , and  $E$  is discussed further in the Appendix.

## 2.2 Lateral interaction energies

When Cl ions adsorb on the surface, a fraction of their charge is transferred through the external circuit. This fraction,  $\epsilon$ , is negative and is directly related to the average resident charge per ion,  $q = (1 + \epsilon)e$  [2]. This relationship is an approximation and is more valid as the potential at the adsorbate approaches the value of the potential in the solution. For the current system's ionic strength, this condition is only approximately satisfied and may be considered as a source of error.

We have previously shown [3] that for Cl/Ag(100), the electrosorption valency depends on the coverage, which is defined as

$$\bar{\gamma} = N^{-1} \sum_{i=1}^{N^2} c_i : \quad (4)$$

In order to investigate such a dependence more thoroughly, we here propose a model with a coverage-dependent next-nearest-neighbor lateral interaction energy  $\epsilon_{nnn}$ , as well. This is motivated by two assumptions: that  $\bar{\gamma}$  is coverage dependent and that the major contribution to  $\epsilon_{nnn}$  is due to electrostatic dipole-dipole interactions. A simple electrostatic picture of the adlayer, in which an adsorbate's resident charge and its image charge form a dipole, suggests a relationship between the electrosorption valency and the dipole moment. If  $\bar{\gamma}$  is coverage dependent ( $\bar{\gamma} = \bar{\gamma}(\bar{\gamma})$ ), then the resident charge is also coverage dependent ( $q = q(\bar{\gamma})$ ), and hence  $\epsilon_{nnn}$ , which is proportional to  $q^2$ , is coverage dependent as well ( $\epsilon_{nnn} = \epsilon_{nnn}(\bar{\gamma})$ ).

Assuming for simplicity that  $\bar{\gamma}$  depends linearly on  $\bar{\gamma}$ ,

$$\bar{\gamma} = \bar{\gamma}_0 + \bar{\gamma}_1 \bar{\gamma} ; \quad (5)$$

the resident charge  $q$  becomes

$$q = (1 + \bar{\gamma}_0 + \bar{\gamma}_1 \bar{\gamma})e ; \quad (6)$$

and  $n_{nnn}$  takes the form :

$$n_{nnn} = A (1 + \alpha_0 + \alpha_1)^2; \quad (7)$$

where  $A$  is a prefactor proportional to the square of a "dipole distance". If  $\alpha$  is coverage independent (i.e.,  $\alpha_1 = 0$ ), then  $n_{nnn}$  becomes coverage independent, as well.

### 2.3 Monte Carlo method

Equilibrium Monte Carlo (MC) simulations were used to measure the equilibrium coverage as a function of  $\bar{r}$ , which was then converted to  $E$  using Eq. (3). At each MC step a lattice site,  $i$ , was chosen randomly, and a change in its occupation variable  $c_i$  was attempted with a Metropolis acceptance probability [16]:

$$R = \min(1, \exp \frac{H}{k_B T}); \quad (8)$$

where  $H$  is the energy difference between the initial state and the proposed state. The value of  $n_{nnn}$  was updated in the simulations at each MC step, corresponding to the new proposed coverage.

The energy difference  $H$  was calculated from Eq. (1) using two methods, a truncated sum of the contributions of neighboring occupied sites up to five lattice spacings away [2, 3, 6], and a mean-field-enhanced truncated sum up to three lattice spacings [3]. In the latter method, energy contributions from adparticles more than three lattice spacings away are calculated using a mean-field estimate as detailed in Ref. [3].

## 3 Experimental

A detailed description of the experimental procedure is given in Ref. [3, 8], and only a brief summary follows here. The Ag(100) single-crystal electrodes were chemically etched in cyanide solution, rinsed in Milli-Q water, and carefully annealed in a hydrogen flame. They were then quickly transferred into the electrochemical cell after cooling in a stream of Argon. Using the hanging meniscus technique, a platinum wire counter electrode, and a saturated calomel electrode as reference electrode, the electrochemical measurements were carried out at a temperature of 20 ± 1 °C.

For the chronocoulometric experiments, the potential was set at initial values between 1.375 and 0.300 V vs SCE until adsorption equilibrium was established, and then stepped to the final potential of 1.400 V, where the chloride is completely desorbed from the surface.

## 4 Results

The equilibrium MC simulations were performed at a temperature of 17 C for various values of  $A$ ,  $\alpha_0$ , and  $\alpha_1$ . The value of  $A$  was varied from 0 to 100 m eV in steps of 5 m eV, while  $\alpha_0$  and  $\alpha_1$  were varied from 0 to 0.9 in steps of 0.1, resulting in 2000 different simulations. The resulting simulated isotherms were fitted to experimental data. This large number of simulations necessitated the choice of the relatively small system size with  $L = 32$ . The system displays a second-order phase transition from a disordered, low-density phase to an ordered c(2 2) phase [2] at an intermediate value of the electrochemical potential. For the steepest part of the isotherm (Fig. 2), where critical slowing down due to the phase transition is important, the system was allowed to relax for a longer time to reach equilibrium than for the points further away from the phase transition. We checked for finite-size effects, and no significant difference was observed when comparing the resulting isotherms with isotherms simulated using larger system sizes of  $L = 64, 128$ , and 256. A small value of  $L$  can be used because  $\gamma$  is not the order parameter corresponding to the c(2 2) phase, and so its fluctuations, which are proportional to  $d = L$ , only diverge logarithmically with  $L$  [2, 17, 18]. In addition, better statistics were collected close to the phase transition, using longer runs and more sampling than for points far from the phase transition, where the fluctuations are smaller.

Using Eq. (3), the simulated isotherms were converted from the  $\bar{\gamma}$  scale to the  $\gamma$  scale and then fit to the experimental isotherms. The fitting was done by varying the value of  $\gamma_0$  to minimize  $\chi^2$  for each set of values for  $A$ ,  $\alpha_0$ , and  $\alpha_1$ . Here,

$$\chi^2 = \frac{\sum_{\text{exp points}} (\gamma_{\text{exp}} - \gamma_{\text{sim}})^2}{\text{degrees of freedom}} \quad (9)$$

$\chi^2$  is the least-squares sum per degree of freedom, and  $\gamma_{\text{exp}}$  and  $\gamma_{\text{sim}}$  are the experimental and simulated coverages, respectively, corresponding to the same value of  $\gamma$ . Linear interpolation was used between the simulated data points

to calculate  $\hat{\gamma}_2$  for all values of  $E$ .

From  $t_s$  to  $10 \text{ mM}$  and  $20 \text{ mM}$  experiments, a grid of values of  $\hat{\gamma}_2$  was collected. Three different models were studied. (i) A constant (i.e., also constant  $\gamma_{nnn}$ ) model for which we only considered the simulations with  $\gamma_1 = 0$ . (ii) A model in which only the line with  $\gamma_0 = 0.3$ ;  $\gamma_1 = 0.3$  was considered. These values for  $\gamma_0$  and  $\gamma_1$  were estimated from values of obtained from the experimental data in Ref. [3] using the method in Ref. [19]. (iii) The third model studied was the coverage dependent model with  $\gamma_{nnn} = \gamma_{nnn}(\gamma_0)$ , where no constraints on the values of any of the parameters were imposed, and the whole parameter space was searched for a global minimum.

A three-dimensional plot of the parameter space is shown in Fig. 3(a), where the diameters of the symbols are proportional to  $1 = \hat{\gamma}_2$  for  $t_s$  to  $20 \text{ mM}$  (circles) and  $10 \text{ mM}$  (squares) of the mean-field-enhanced simulations. The parameter space for the non-mean-field-enhanced method (not shown) is similar. Figure 3(a) shows the existence of several local minima and a good overlap between the minima for both concentrations. The position of the accepted global minimum is indicated by the arrows. Figure 3(b) is a projection onto the  $\gamma_0, \gamma_1$  plane, which shows that the minima are concentrated within one region close to the  $\gamma_1 = 0$  plane, suggesting a relatively weak dependence of  $\hat{\gamma}_2$  on the coverage. Moreover, the  $\hat{\gamma}_2$  values in the  $\gamma_1 = 0$  plane (model (i)) and for  $\gamma_0 = \gamma_1 = 0.3$  (model (ii)) are significantly larger than the  $\hat{\gamma}_2$  values for the accepted global minimum (model (iii)). Figures 3(c) and 3(d) show that while the magnitude of  $\gamma_0$  decreases monotonically with increasing  $A$ , there is no general trend for  $\gamma_1$  as a function of  $A$ .

Due to the existence of several shallow minima of  $\hat{\gamma}_2$ , and due to the limited resolution of the grid in parameter space, we list in Table 1 the best-fit parameter values for each model, along with all  $t_s$  that have  $\hat{\gamma}_2$  within 10% of the best-fit value. One can see in Table 1 that there are two possible sets of parameters that fit to the  $10 \text{ mM}$  data for model (iii) with mean-field-enhanced simulations. To discriminate between these possible fits to the  $10 \text{ mM}$  data we check if they are also possible fits to the  $20 \text{ mM}$  experimental data. The first set ( $A = 90 \text{ meV}$ ) is the overall best fit for  $10 \text{ mM}$ . However, it is only slightly better than the second set ( $A = 55 \text{ meV}$ ), and it is not a possible fit to the  $20 \text{ mM}$  experimental data. The only parameter set ( $A = 55 \text{ meV}$ ,  $\gamma_0 = 0.4$ ,  $\gamma_1 = 0.2$ ) that is a possible fit to both the  $10 \text{ mM}$  and  $20 \text{ mM}$  experimental data, is the accepted best fit for model (iii). Using the same approach for the non-mean-field-enhanced method, models

(i) and (ii), and concentration, results in a unique set of parameter values for each model, simulation method, and concentration. These accepted ts are summarized in Table 2. Notice in Table 2 that for the accepted global minimum of model (iii), and for both mean-field-enhanced and non-mean-field-enhanced methods, the values of  $\sigma_0$  and  $\sigma_1$  are reasonably close to the ones calculated from the experimental data [3] using the method of Ref. [19]. Also note that the ts for 10 mM are consistently better than the ts to the 20 mM experiments. This might be due to violation of the dilute-solution limit at the higher concentration. This may also be the reason that the values of  $\sigma_0$ , which are expected to be the same for both concentrations when  $\sigma$  to a single simulation, differ consistently by about 12–7 meV between the concentrations. The values of  $A$  are consistently less negative for the longer-ranged lateral interactions of the mean-field-enhanced than for the non-mean-field method. This is not surprising.

The quality of the ts is better for model (iii), as can be seen from the plots corresponding to each of the models (Figs. 2, 4 and 5). Models (ii) and (iii) fit worse at either the lower-coverage part of the isotherm (model (ii)), see Fig. 4, or at the upper part of the isotherm (model (i)), see Fig. 5. In contrast, the best-fit simulations in Fig. 2 fit the experiments well over the whole range of coverages. The plots for the non-mean-field-enhanced ts (not shown) are similar. A plot of  $\sigma$  vs  $E$  is shown in Fig. 6(a) for the best-fit values of  $\sigma_0$  and  $\sigma_1$  corresponding to the 10 mM experimental data for each of the three models considered. Also shown are the values of  $\sigma$  obtained in Ref. [3] by the method of Ref. [19]. While model (ii) is expected to fit the Ref. [3, 19] values of  $\sigma$ , model (i) also predicts a value of  $\sigma$  close to, but slightly more negative than, the mean of the values of  $\sigma$  from Ref. [3, 19]. The  $\sigma_{nnn}$  values corresponding to the best ts of the three models are shown in Fig. 6(b).

Since the ts are sometimes better for the mean-field-enhanced method, and sometimes worse, the mean of the sets of parameters obtained by including and excluding the mean-field enhancement are reported here as our final results:  $A = -60$  meV;  $\sigma_0 = 0.4$ ;  $\sigma_1 = 0.2$ , and  $\sigma_0 = 325$ . In the far-field approximation used here, the lateral interaction energy between two parallel dipoles separated by a distance  $a/2$  is given by

$$\sigma_{nnn} = \frac{1}{4} \frac{p^2}{\sigma_0 (a/2)^3} = A (1 + \sigma_0 + \sigma_1)^2 = A \frac{q^2}{e^2}; \quad (10)$$

where  $p = qd$  is the dipole moment,  $d$  is an effective "dipolar distance," and

the second and third equalities result from Eqs. (7) and (6), respectively. Consequently,

$$p = \frac{q}{e} \frac{q}{4} \frac{p}{\epsilon_0 (a/2)^3 A} \quad (11)$$

For the  $A = 60 \text{ m eV}$  final result, the dipole moment ranges between  $p = 0.32 \text{ eA}$  for  $a = 0$  and  $p = 0.26 \text{ eA}$  for  $a = 0.5$ , and the "dipolar distance"  $d = 0.53 \text{ \AA}$ . Density Functional Theory calculations of a model without water [20] suggest a dipole moment of  $0.46 \text{ eA}$ , which is only about 40% higher than the fitted value at low coverage. However, from simple physical intuition, the dipolar distance might be expected to be of the order of the ionic diameter of  $\text{Cl}^-$ , about  $3 \text{\AA}$ . The value of  $d$  obtained here involves several assumptions. One main assumption used is that the dipole is a classical point dipole, which should be quite reasonable as the distance between neighboring dipoles is about an order of magnitude larger than the obtained value for  $d$ . Moreover, we have assumed that the interaction is a classical electrostatic dipole interaction, while there could be quantum effects at the shortest length scales. On the other hand, when viewed as a charge distribution, the dipole is expected to have a much smaller "dipolar distance" than naively expected [21]. Using the relationship between the dipole moment and the Helmholtz capacitance  $C_H$  [22],

$$p = qd = \frac{\epsilon_0}{C_H} (1 + \dots); \quad (12)$$

and our values for the dipole moment and  $C_H$ , we obtain a  $C_H$  that is in the range of 26 to 32  $\text{F/cm}^2$ . This range is comparable to the reported value of  $C_H$  for  $\text{Ag}(110)$  in chloride ion solution  $C_H = 100 \text{ F/cm}^2$  [21], which would yield  $d = \epsilon_0 C_H = 0.1 \text{ \AA}$ . This value of  $d$  is consistent with our value.

Finally, although models (i) and (ii) are still possible, a self-consistent (non- $\epsilon$  model) entirely electrostatic model not only fits better to the experimental data but also, with no constraints imposed, predicts values of  $d$  that are reasonably compatible with those obtained from the experimental data using the method of Ref. [19].

## 5 Conclusion

A discrepancy between values of the electrosorption valency obtained from fitting simulations to experiments, and the value obtained from the analysis [19] of experimental data was reported in a previous study by Abou

Huang et al. [3]. This discrepancy suggested that the long-range interactions are dominated by electrostatic dipole/dipole effects for C1 electrosorption on the Ag(100) single crystal surface.

In this work, a large set of MC simulations (2000 simulations) over a grid in parameter space was fitted to two sets of chronocoulometry experimental data for different concentrations. The existence of local minima of  $\chi^2$  in parameter space suggests alternative models. To within the resolution of our grid and the accuracy of the experimental data, we have shown that while other, simpler, models are still possible, a purely electrostatic model can be used to describe the C1/Ag(100) system. It also predicts an electrosorption valency that is compatible with the value obtained through direct experimental data analysis by the method of Ref. [19]. Additional sets of experimental data, with different concentrations around 10 and 20 mM of the adsorbate ion, along with a finer grid in parameter space would enable a more decisive determination of the most appropriate model and its parameter values.

## Acknowledgments

We thank S. Frank and M. T. M. Koper for useful discussions and helpful comments. This work was supported in part by NSF grant No. DMR-0240078, and by Florida State University through the School of Computational Science and the Center for Materials Research and Technology, the Research Centre Jülich, and the Shuit Institute for Catalysis, Technical University of Eindhoven, The Netherlands.

## Appendix

In this appendix we discuss the relationship between the electrochemical potential  $\varphi$  and the electrode potential  $E$  for a coverage or field dependent electrosorption valency  $\gamma$ .

We define the electrosorption valency as [22]

$$\gamma = \frac{\varphi_M - \varphi_E}{\varphi_M}; \quad (13)$$

where  $\varphi_M$  is the charge on the metal,  $\gamma$  is the coverage, and  $\varphi_E$  is the chemical potential of the solution (here taken as the dilute-solution approximation,

$= k_B T \ln \left( \frac{C}{C_0} \right)$ . Considering an auxiliary thermodynamic potential  $X$  related to the surface tension as

$$X = \dots + \dots ; \quad (14)$$

and using the Lippmann equation,

$$dX = d \underset{M}{\text{d}E} ; \quad (15)$$

we have

$$\frac{\partial X}{\partial E} \underset{M}{=} \text{d}E \text{ and } \frac{\partial X}{\partial \epsilon} \underset{M}{=} \text{d}E ; \quad (16)$$

Consequently, one obtains the Maxwell relation, [22]

$$= \frac{\frac{\partial \underset{M}{\text{d}E}}{\partial \epsilon}}{E} = \frac{\partial X}{\partial E \partial \epsilon} = \frac{\partial}{\partial E} \underset{M}{\text{d}E} ; \quad (17)$$

The relation,  $= \frac{\partial}{\partial E}$ , gives the electroosorption valency as the change in necessary to keep constant under a change in  $E$ . But to keep constant, the electrochemical potential  $\mu$  must remain constant, so that

$$= \frac{\partial}{\partial E} \underset{M}{\text{d}E} \underset{M}{=} \frac{\partial}{\partial E} \underset{M}{\text{d}E} ; \quad (18)$$

It is easy to show that Eq. (3) satisfies this requirement for  $\mu$ . If

$$= -_0 + k_B T \ln \frac{C}{C_0} \underset{E_0}{e}^{Z_E} (E^0) dE^0 ;$$

then

$$= -_0 + \underset{E_0}{e}^{Z_E} (E^0) dE^0 + \text{const.} ; \quad (19)$$

and

$$\frac{\partial}{\partial E} \underset{M}{\text{d}E} \underset{M}{=} \frac{\partial}{\partial E} \underset{M}{\text{d}E} = \underset{M}{\text{d}E} ; \quad (20)$$

Generalization to multiple adsorbates is straightforward.

## References

- [1] T.L. Einstein, in: W.N. Unertl (Ed.), *Handbook of Surface Science*, vol. 1, Elsevier Science B.V., Amsterdam, 1996, p. 577-650.
- [2] S.J.M. Mitchell, G. Brown, P.A. Rikvold, *Surf. Sci.* 471 (2001) 125.
- [3] I. Abou Hamad, Th. W andlowski, G. Brown, P.A. Rikvold, *J. Electroanal. Chem.* 554-555 (2003) 211.
- [4] I. Abou Hamad, P.A. Rikvold, G. Brown, *Surf. Sci.* 572 (2004) L355.
- [5] O. Endo, M. Kiguchi, T. Yokoyama, M. Ito, and T. Ohta, *J. Electroanal. Chem.*, 473 (1999) 19.
- [6] S.J.M. Mitchell, G. Brown, P.A. Rikvold, *J. Electroanal. Chem.* 493 (2000) 68.
- [7] B.M. Ocko, J.X. Wang, Th. W andlowski, *Phys. Rev. Lett.* 79 (1997) 1511.
- [8] Th. W andlowski, J.X. Wang, B.M. Ocko, *J. Electroanal. Chem.* 500 (2001) 418.
- [9] O.M. M agnussen, *Chem. Rev.* 102 (2002) 679.
- [10] G. Valette, A. Hamelin, R. Parsons, *Z. Phys. Chem. Neue Fol.* 113 (1978) 71.
- [11] Th. W andlowski, B.M. Ocko, J.X. Wang, *in preparation* (2005).
- [12] S.J.M. Mitchell, S.W. Wang, P.A. Rikvold, *Faraday Disc.* 121 (2002) 53.
- [13] M.T.M. Koper, *J. Electroanal. Chem.* 450 (1998) 189.
- [14] M.T.M. Koper, *Electrochim. Acta* 44 (1998) 1207.
- [15] K.J. Vetter, J.W. Schultze, *Ber. Bunsenges. Phys. Chem.* 76 (1972) 920; *ibid* 76 (1972) 927.
- [16] D.P. Landau, K.B. Binder, *A Guide to Monte Carlo Simulations in Statistical Physics*, Cambridge Univ. Press, Cambridge, 2000.

- [17] K. Binder, *Ann. Rev. Phys. Chem.* 43 (1992) 33.
- [18] P A . R ikvold, *Phys. Rev. B* 32 (1985) 4756; *Erratum : Phys. Rev. B* 33 (1986) 6523.
- [19] J. Lipkowski, J. Stolberg, in: J. Lipkowski, P N . Ross, (Eds.), *Adsorption of Molecules at Metal Electrodes*, VCH Publishers, New York, 1992, pp. 171-238.
- [20] I. Abou Hamad, S J. M itchell, unpublished.
- [21] W . Schmidkler, *J. Electroanal Chem.* 249 (1988) 25.
- [22] W . Schmidkler, *Interfacial Electrochemistry*, Oxford Univ. Press, New York Oxford, 1996, Chapter 18.

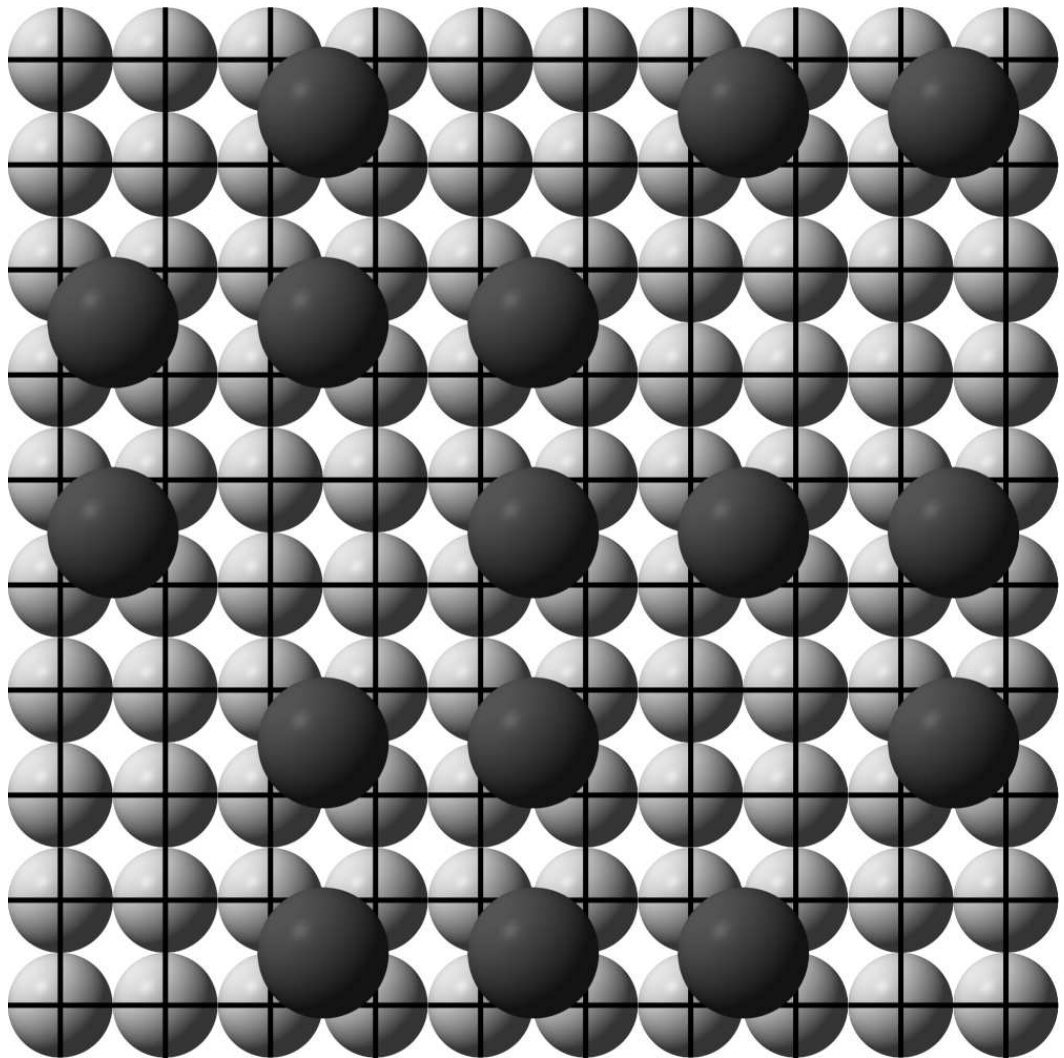


Figure 1: C 1 (larger, dark gray, spheres) adsorbed at the 4-fold hollow sites of the (100) surface of Ag (smaller, lighter gray, spheres). The grid frame corresponds to the lattice of adsorption sites. The figure is drawn approximately to scale.

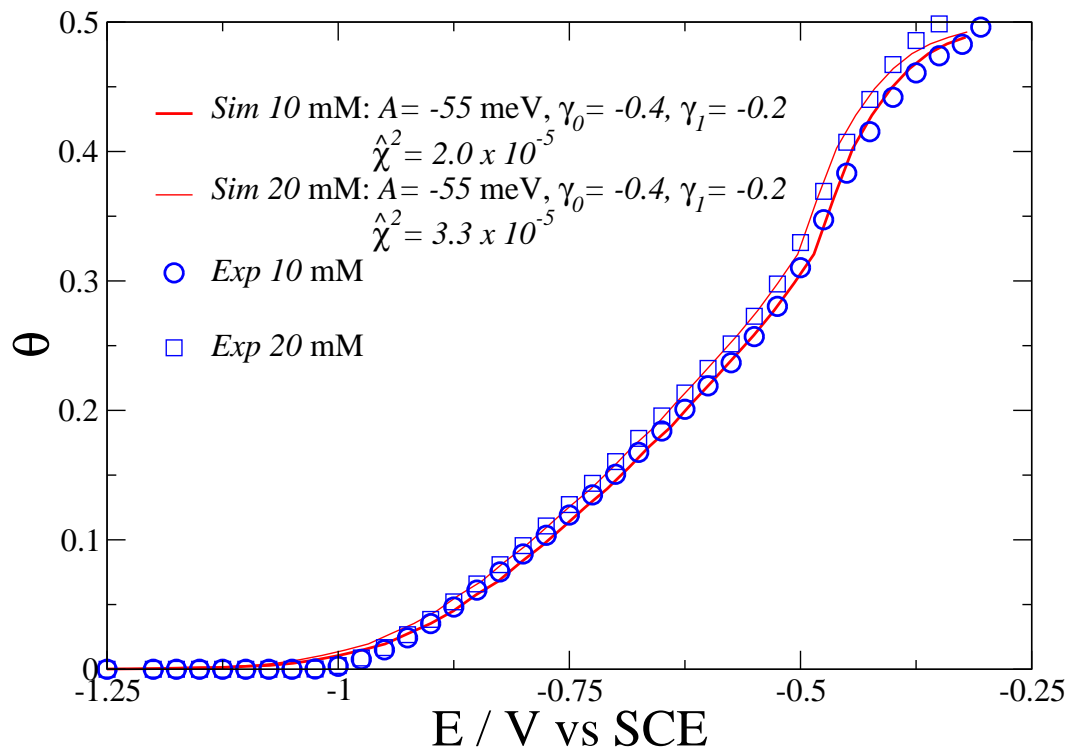


Figure 2: Best fit of mean-field-enhanced simulation to experimental 10 mM and 20 mM coverage isotherms:  $A = -55 \text{ meV}$ ,  $\gamma_0 = -0.4$ ; and  $\gamma_1 = -0.2$  (model (iii)).  $L = 32$ .

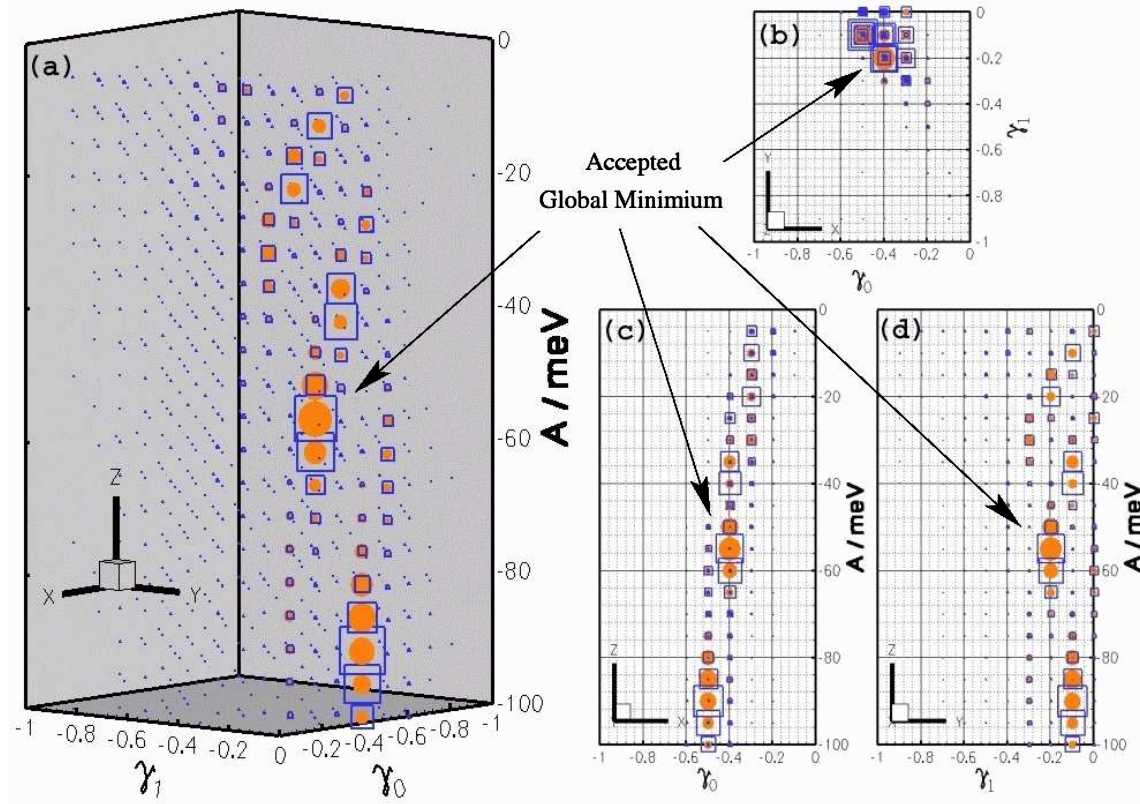


Figure 3: A plot of  $1 - \gamma^2$  in the three-dimensional parameter space, obtained from fits of mean-field-enhanced simulations to the 10 mM experimental data (squares) and the 20 mM experimental data (circles). The diameters of the symbols are proportional to  $1 - \gamma^2$ . (a) is a three-dimensional view, (b) is a projection onto the  $\gamma_0, \gamma_1$  plane, and (c) and (d) are projections onto the  $\gamma_0, A / \text{meV}$  plane and the  $\gamma_1, A / \text{meV}$  plane respectively. The parameter space for the non-mean-field-enhanced method (not shown) is similar.

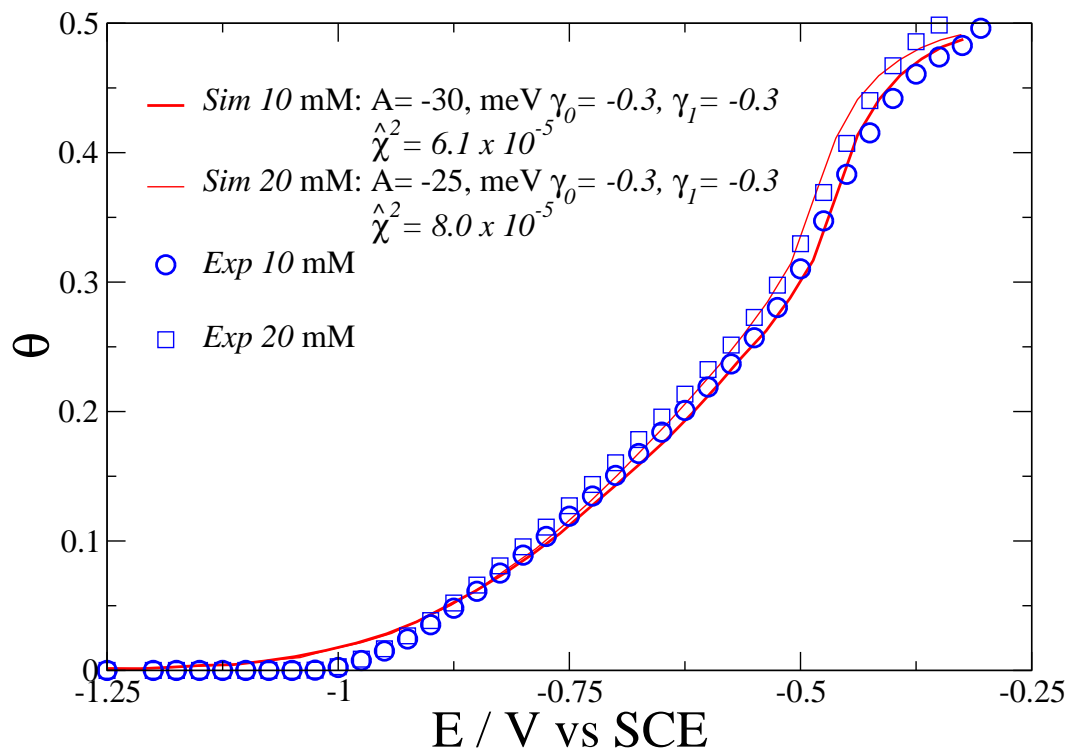


Figure 4: Simulated constrained best fit with the values of  $\gamma_0 = -0.3$  and  $\gamma_1 = -0.3$  (model (ii)) for the 10 and 20 mM experimental data. Mean-field-enhanced simulations are shown here.  $L = 32$ .

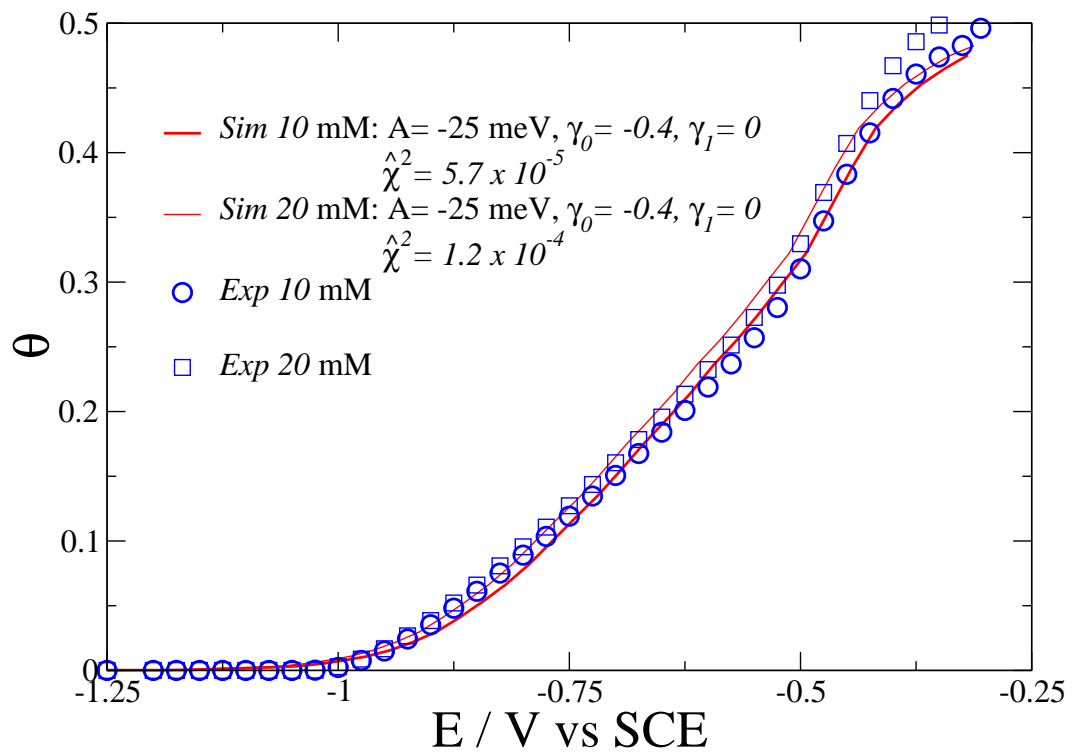


Figure 5: Simulated constrained best fit with a constant  $\gamma_I$  (model (i)) for the 10 and 20 mM experimental data. Mean-field-enhanced simulations are shown here.  $L = 32$ .

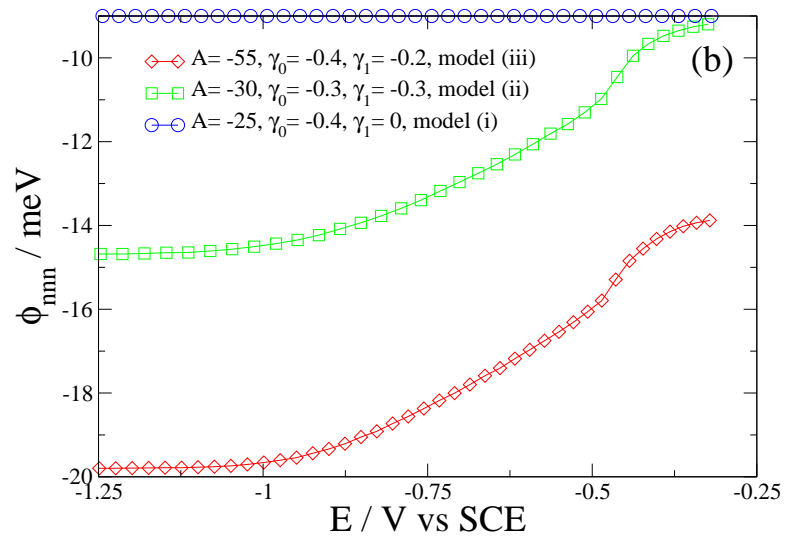
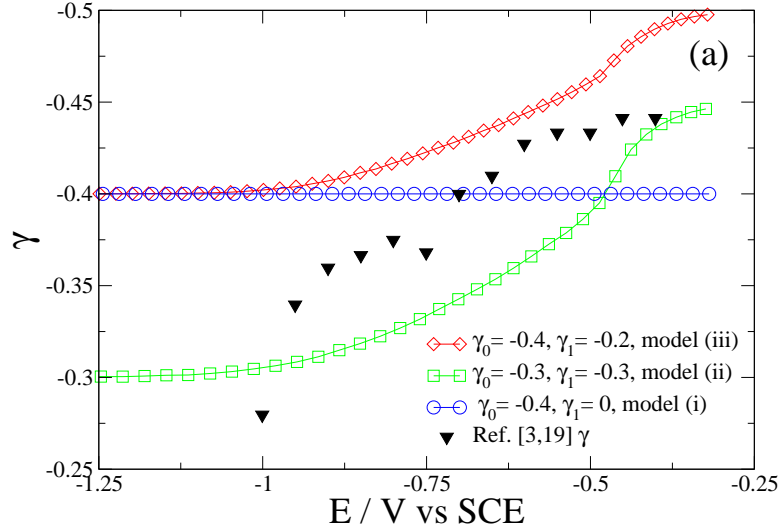


Figure 6: (a) The electrosoption valency  $\gamma$  vs  $E$  for the values of  $\gamma_0$  and  $\gamma_1$  obtained from the best fits for models (i), (ii), and (iii) to the 10 mM experimental data. The values of  $\gamma$  obtained in Ref. [3] by the method of Ref. [19] are also shown. (b) Corresponding plots of  $\phi_{nnn}$  vs  $E$  for the three models.

Table 1: Fitting parameters for Cl adsorption on a Ag(100) single-crystal surface, for models (i), (ii), and (iii), with and without mean-field interactions. Possible fits to within 10% of the best  $\chi^2$  for each model are also shown.  $A$  and  $\gamma_0$  are in units of meV.

Model	Mean-field enhanced										
	10 mM					20 mM					
	$A$	$\gamma_0$	$\gamma_1$	$\gamma_0$	$\chi^2 \cdot 10^5$		$A$	$\gamma_0$	$\gamma_1$	$\gamma_0$	$\chi^2 \cdot 10^5$
(i) Const.	25	0.4	0	330	5.664		60	0.5	0	390	11.927
	5	0.3	0	281	5.769		55	0.5	0	396	11.942
							25	0.4	0	340	12.079
							20	0.4	0	349	12.514
(ii) Ref. [3, 19]	30	0.3	0.3	266	6.068		25	0.3	0.3	285	8.037
(iii) $nnn( \langle \rangle )$	90	0.5	0.1	371	1.815		55	0.4	0.2	328	3.340
	55	0.4	0.2	318	1.976						
No mean-field enhancement											
(i) Const.	30	0.4	0	330	5.369		70	0.5	0	393	11.246
							30	0.4	0	341	11.330
							65	0.5	0	398	11.350
							25	0.4	0	348	11.606
(ii) Ref. [3, 19]	35	0.3	0.3	268	6.086		30	0.3	0.3	286	7.462
(iii) $nnn( \langle \rangle )$	45	0.4	0.1	325	2.310		65	0.4	0.2	330	3.112
	65	0.4	0.2	320	2.311						

Table 2: The best-fit parameters for Cl adsorption on a Ag(100) single-crystal surface, for models (i), (ii), and (iii), with and without mean-field interactions.  $A$  and  $\gamma_0$  are in units of meV.

Model	Mean-field enhanced										
	10 mM					20 mM					
	$A$	$\gamma_0$	$\gamma_1$	$\gamma_0$	$\chi^2 \cdot 10^5$		$A$	$\gamma_0$	$\gamma_1$	$\gamma_0$	$\chi^2 \cdot 10^5$
(i) Const.	25	0.4	0	330	5.664		25	0.4	0	340	12.079
	30	0.3	0.3	266	6.068		25	0.3	0.3	285	8.037
	55	0.4	0.2	318	1.976		55	0.4	0.2	328	3.340
No mean-field enhancement											
(i) Const.	30	0.4	0	330	5.369		30	0.4	0	341	11.330
	35	0.3	0.3	268	6.086		30	0.3	0.3	286	7.462
	65	0.4	0.2	325	2.310		65	0.4	0.2	330	3.112